ADVANCED MATERIALS
www.advmat.de

Nature-Inspired Nacre-Like Composites Combining Human Tooth-Matching Elasticity and Hardness with Exceptional Damage Tolerance

Guoqi Tan, Jian Zhang, Long Zheng, Da Jiao, Zengqian Liu, Zhefeng Zhang,* and Robert O. Ritchie**

Making replacements for the human body similar to natural tissue offers significant advantages but remains a key challenge. This is pertinent for synthetic dental materials, which rarely reproduce the actual properties of human teeth and generally demonstrate relatively poor damage tolerance. Here new bioinspired ceramic–polymer composites with nacre-mimetic lamellar and brick-and-mortar architectures are reported, which resemble, respectively, human dentin and enamel in hardness, stiffness, and strength and exhibit exceptional fracture toughness. These composites are additionally distinguished by outstanding machinability, energy-dissipating capability under cyclic loading, and diminished abrasion to antagonist teeth. The underlying design principles and toughening mechanisms of these materials are elucidated in terms of their distinct architectures. It is demonstrated that these composites are promising candidates for dental applications, such as new-generation tooth replacements. Finally, it is believed that this notion of bioinspired design of new materials with unprecedented biologically comparable properties can be extended to a wide range of material systems for improved mechanical performance.

G. Tan, J. Zhang, Dr. D. Jiao, Prof. Z. Liu, Prof. Z. Zhang
Laboratory of Fatigue and Fracture for Materials
Institute of Metal Research
Chinese Academy of Sciences
Shenyang 110016, China
E-mail: zengqianliu@imr.ac.cn; zhfzhang@imr.ac.cn
G. Tan, Prof. Z. Liu, Prof. Z. Zhang
School of Materials Science and Engineering
University of Science and Technology of China
Hefei 230026, China
Dr. L. Zheng
Key Laboratory of Bionic Engineering (Ministry of Education)
College of Biological and Agricultural Engineering
Jilin University
Changchun 130022, China
Prof. R. O. Ritchie
Department of Materials Science and Engineering
University of California Berkeley
Berkeley, CA 94720, USA
E-mail: roritchie@lbl.gov
The ORCID identification number(s) for the author(s) of this article can be found under https://doi.org/10.1002/adma.201904603.

DOI: 10.1002/adma.201904603

It is highly desirable to reproduce the properties of human tissues, such as tooth, bone, and muscle, in man-made systems, specifically for biomedical applications such as implants or tissue replacements. However, materials in the human body have evolved complex architectures in achieving their multifunctionality and, in particular, outstanding combinations of properties which are difficult to replicate.[1–6] The human tooth is an excellent case in point where exceptional mechanical efficiency has been developed by ingenious designs. Human dentin, the inner solid part of tooth covering the interior pulp, is moderately mineralized (with a mineral content of ≈70 wt%) and distinguished by good ductility, fracture toughness, and energy-dissipating capability.[7–9] The dentin is enveloped, through a gradient interfacial connection,[3,10] by a hard and stiff exterior—the tooth enamel, which is hypermineralized (with a mineral content of ≈96 wt%).[10–13] Despite its almost fully ceramic nature, tooth enamel is remarkably resilient and viscoelastic, and can even display self-recovery properties at nano- to micro length scales.[12,13] These characteristics result from its elaborate architecture comprising a minor organic phase occupying the abundant interfaces between highly aligned mineral constituents. Additionally, rather than breaking catastrophically with the initiation of any crack, both dentin and enamel display increasing fracture resistance with crack extension, which is manifest by rising crack-resistance (*R*-curve) behavior.[8–11]

Accordingly, it is important to make dental restorations or replacements as similar as possible to the properties of the human tooth (both dentin and enamel) in order to replicate their biomechanical functions. Nevertheless, this has not been effectively realized in any dental materials to date and still remains a key challenge. There are two critical requirements for ideal tooth replacements in terms of the mechanical properties. First, the dental materials should be comparably hard, stiff, and strong as the human tooth so as to fulfill their mechanical demands. However, immoderately high hardness and Young's modulus may cause excessive damage and accelerated abrasion of the opposing teeth, and are thus undesirable properties.[14–18]

On this basis, tooth replacements are preferred to be damage tolerant and capable of absorbing/dissipating mechanical energy at loading to ensure good durability.

Ceramics, specifically yttria-stabilized tetragonal zirconia polycrystals (Y-TZP), and ceramic-based composites are prominent among various dental restorative materials owing to their high hardness and stiffness, superior biocompatibility, and satisfactory aesthetics.[14,15,19,20] However, these bioceramics are extremely hard and stiff compared to human teeth; for example, Y-TZP is, respectively, ≈4 and ≈24 times harder than human enamel and dentin (the hardness of Y-TZP is ≈12 GPa, whereas the hardness values of human enamel and dentin have been reported to be ≈2.74–3.74 and 0.46–0.65 GPa, respectively).[21,22] Moreover, such materials exhibit distinct brittleness because of their ceramic nature. These properties can lead to unfavorably high flaw sensitivity and an increased tendency for failure of the restorations along with the easy abrasion and damage of antagonist teeth.[14,15,23–25] Additionally, bioceramics invariably exhibit poor machinability, which necessitates personal customized production of tooth replacements, i.e., each replacement must experience an individual sequence of processing.

However, dental materials can be made softer and more compliant by combining ceramics with a glass or polymer phase to form compliant-phase composites.[26–30] It remains unclear though how such composites can be created to be similar to both the dentin and enamel in the human tooth, specifically with respect to their mechanical properties. Indeed, most dental materials to date lack any true architectural design, especially at micro to nano length scales, and are inevitably either harder or softer than the human tooth. Additionally, these materials are generally plagued by minimal fracture toughness, typically lower than 4 MPa $m^{1/2}$ for ceramics (except for the Y-TZP) and glass–ceramics and lower than 2.5 MPa $m^{1/2}$ for ceramic–polymer composites.[14,20,26,28–30] As such, they can rarely reproduce the crack-resistance (*R*-curve) behavior and energy dissipation efficiency of the human tooth.

Taking lessons from nature offers increasing promise for solving the problems encountered by man-made materials.[31–39] Here, we report on the bioinspired design and fabrication of novel ceramic–polymer composites with characteristic hardness and stiffness comparable to those of human dentin and enamel. This is realized by mimicking the structure of nacre in mollusk shells, which is particularly a fracture-resistant yet highly mineralized biological material.[40,41] Besides their similarities with the mechanical properties of the human tooth, these composites exhibit extraordinary damage tolerance in terms of their fracture toughness, *R*-curve behavior, remarkable energy-dissipating capability, good machinability, and diminished abrasion to opposing teeth. Such an unprecedented combination of properties outperforms the benchmark of current dental materials and, consequently, presents an encouraging opportunity for dental applications.

Figure 1a illustrates the formation process and micromechanisms of our nacre-mimetic composites based on tetragonal

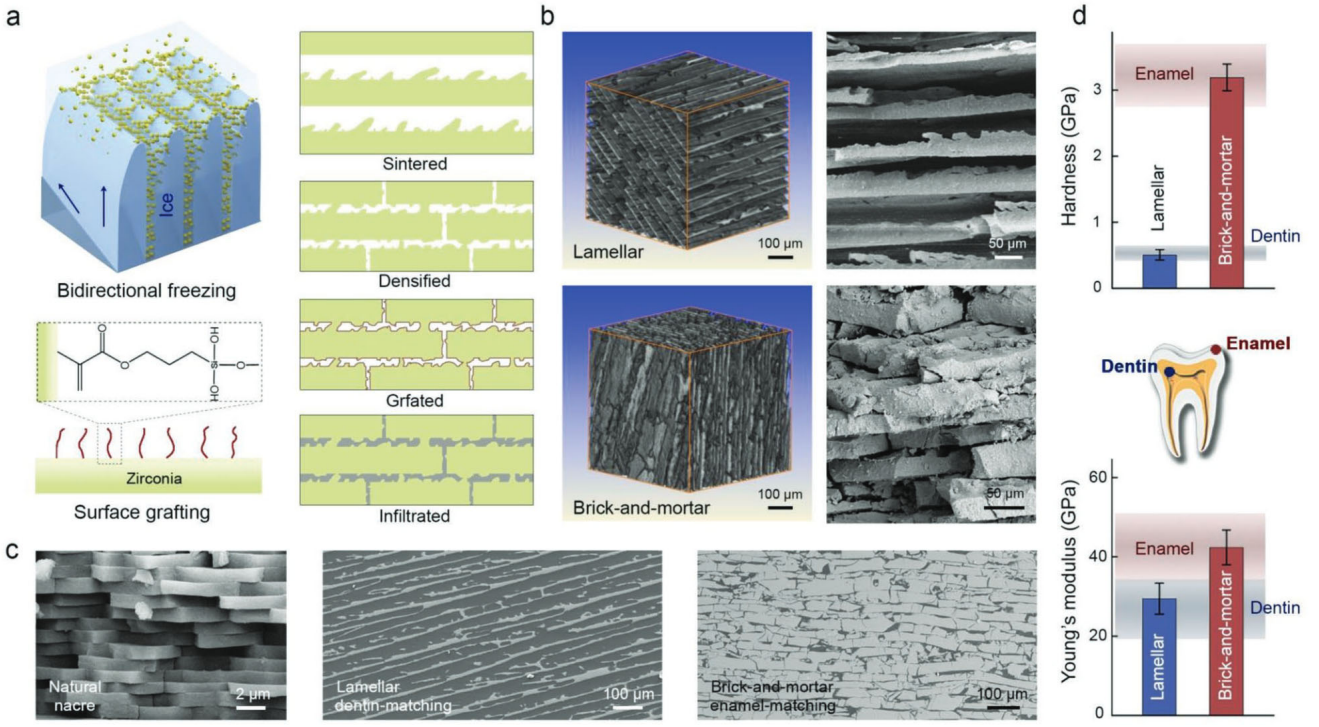

Figure 1. Formation and microstructure of composites with human-tooth-matching hardness and stiffness. a) Schematic illustrations showing the formation process of nacre-mimetic composites and the micromechanisms for bidirectional freeze-casting and surface grafting. b) XRT volume renderings and SEM images of the mineral scaffolds for lamellar and brick-and-mortar composites. c) SEM images of the nacre-mimetic composites with lamellar and brick-and-mortar architectures as compared to natural nacre. d) Comparison of the hardness and Young's modulus of our composites with human dentin and enamel. Here the mechanical data for human tooth were collected from the literature by considering their hydrated state and excluding those determined by nanoindentation, which tends to overestimate the hardness and Young's modulus of bulk samples.

zirconia polycrystals doped with 3 mol% yttria (3Y-TZP). The infiltration of ceramic scaffolds with differing mineral contents produced by freeze-casting and densification with a polymer phase results in composites with nacre-like lamellar and brick-and-mortar architectures. Full details on the fabrication of these composites are given in the Experimental Section. During the bidirectional freezing process, the mineral particles and additives in the suspension are expelled from the growing ice crystals into their microspaces and rearranged into a long-range ordered lamellar structure.[32,39,42,43] This is enabled by the dual temperature gradients formed in the slurry, i.e., the vertical gradient created by the cold finger and the horizontal one generated from the polydimethylsiloxane (PDMS) wedge.[42,43] The subsequent water sublimation and sintering result in porous 3Y-TZP scaffolds with a porosity of ≈80 vol% for the slurry with 35 wt% solid load (Figure 1b). Abundant micro- to nanoscale dendrites and asperities are formed on the mineral lamellae of scaffolds because of the inconsistency between the imposed temperature gradient and crystallographic preferred growth direction of ice crystals during freezing.[32,44] These structures account roughly for one-fifth of total volume of the ceramic phase. Densification of the scaffolds by pressing along the normal direction of mineral lamellae causes their breakage into separate bricks and allows for dense packing of these bricks. The subsequent re-sintering process leads to the formation of mineral bridges and multiple interconnections between adjacent bricks. This results in 3Y-TZP scaffolds with good integrity and a markedly decreased porosity of ≈23 vol% (Figure 1b).

Nacre-mimetic composites can be fabricated by infiltrating the porous 3Y-TZP scaffolds with a clinically used dental resin. Surface grafting of the scaffolds before infiltration with γ-methacryloxypropyltrimethoxysilane (γ-MPS), which is a commonly used surface coupling agent, plays a role in enhancing the interfacial adhesion between the 3Y-TZP and the resin.[39,45] This is achieved by forming covalent bonds between the inorganic and organic components through the reaction of siloxane bonds and hydroxyl groups on the surface of 3Y-TZP. Figure 1c shows the structures of infiltrated composites using different scaffolds, in comparison to natural nacre of the *Sinanodonta woodiana* mollusk shell.[46] Despite the differing characteristic dimensions, volume fractions, and types of constituents compared to nacre, the composites replicate, to a large extent, the architectural designs of nacre in terms of their alternating arrangement of organic and inorganic phases in a laminated fashion and the micro- to nanoscale bridges and asperities of the mineral layers. Specifically, a nacre-like lamellar structure is formed in composites with relatively low (≈20 vol%) mineral content; by comparison, the infiltration of densified scaffolds leads to the formation of a brick-and-mortar architecture possessing a high mineral content up to ≈77 vol% with the interspace between 3Y-TZP bricks filled with resin.

The layer thickness of the mineral is between 4 and 12 μm and between 10 and 25 μm for the lamellar and brick-and-mortar composites, respectively; such a difference is principally associated with the differing solid load in the slurry during freeze-casting. The mineral bricks in the latter are staggered between adjacent layers; they have a length of 70–160 μm with an average aspect ratio of ≈6.8. The interlayer polymer phase displays a characteristic thickness of tens of micrometers in the lamellar composites and several sub-micrometers in the brick-and-mortar materials. The distinctly different constitution and architectures of these composites endow them with unique hardness and Young's modulus which are closely comparable to, respectively, those of human dentin and enamel, as shown in Figure 1d.

Figure 2a presents typical stress–strain curves of the nacre-mimetic lamellar and brick-and-mortar composites under monotonic and cyclic compression—the latter resembles the actual loading state of teeth. Both composites display compressive strengths over 350 MPa and apparent deformation exceeding 1% before failure. In particular, their mechanical properties are characterized by hysteresis stress–strain loops under cyclic loading–unloading conditions. Such features result essentially from the viscoelastic and plastic nature of the composites endowed by the polymer component, which provides an effective means for absorbing or dissipating the imposed mechanical energy. This is reminiscent of the viscosity of human enamel and dentin which plays a key role in achieving the exceptional durability of the tooth to accomplish its biomechanical function.[9,12,13]

The Young's moduli of the lamellar and brick-and-mortar composites, as determined by the slope of the linear region on their stress–strain curves, are 29 ± 4 and 42 ± 4 GPa, respectively. These values are between the upper and lower bounds of conventional rule-of-mixtures defined by the Voigt and Reuss models (Figure 2b). The moduli of the composites are markedly lower than that of the monolithic 3Y-TZP ceramic which is over 200 GPa, i.e., 3Y-TZP is almost five and seven times stiffer than that of human enamel and dentin (the Young's moduli of human enamel and dentin have been reported to be ≈30–47 and ≈19–34 GPa, respectively).[47–50] The nacre-like architectures allow for a good matching between the lamellar composites and human dentin as well as between the brick-and-mortar composites and human enamel in terms of their Young's moduli. The theoretical principles underlying such quantitative designs can be understood based on an equivalent element body approach and tension–shear chain model of composites, as will be discussed in the following section. Additionally, similar to the stiffness, the hardness of these nacre-mimetic composites presents a close resemblance to that of the human tooth. The polymer phase plays an effective role in arresting the propagation of cracks away from the mineral lamellae and bricks (Figure 2c), thereby preventing the extension of indentation damage over large dimensions.

In vitro wear tests with bovine teeth reveal a marked decrease in the coefficient of friction (CoF) for the composites as compared to the 3Y-TZP ceramic (Figure 2d). The CoFs of the composites demonstrate a dependence on the orientation of the mineral layers with respect to the sliding direction. The lamellar composites display a lower CoF in the transverse configuration where the sliding motion is perpendicular to the mineral layers as compared to the longitudinal configuration; the brick-and-mortar composites present the opposite trend. Such a difference is presumed to result from the lubricating effect of the polymer phase in mitigating friction which is closely associated with their respective composite architectures. The alternative arrangement of mineral and polymer phases in the lamellar composites enables the introduction of polymer lubricant over

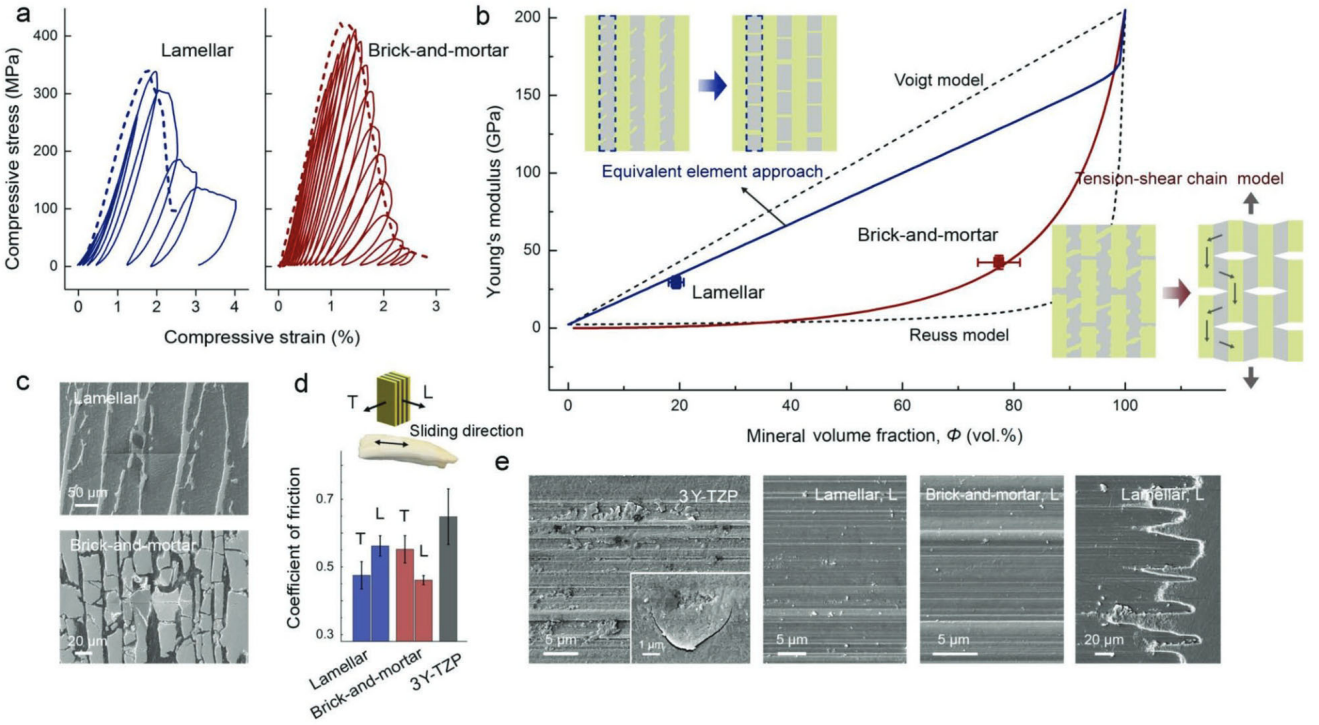

Figure 2. Mechanical properties and wear behavior with bovine teeth of nacre-mimetic composites. a) Compressive stress–strain curves of the lamellar and brick-and-mortar composites under monotonic (dashed) and cyclic (solid) loading conditions. b) The Young's moduli of our composites as a function of the volume fraction of minerals. The insets illustrate the equivalent element body approach and tension–shear chain model for lamellar and brick-and-mortar composites. c) SEM images of the indentation impressions in composites showing limited damage extension. d) Coefficients of friction (CoFs) with antagonist bovine teeth for nacre-mimetic composites along the longitudinal (*L*) and transverse (*T*) directions, as compared to monolithic 3Y-TZP ceramic. Here, the CoFs were determined as the average between 1000 and 3000 cycles of sliding motion where the data present a plateau. e) Representative wear morphologies of bovine teeth in contact with 3Y-TZP and nacre-mimetic composites and one end of wear track for the lamellar composites in the longitudinal configuration (see Figure S2 in the Supporting Information for the CoFs with wear cycles and wear morphologies for the transverse configuration).

the entire contact area of friction along the transverse direction; this contrasts to the case of longitudinal configuration where the mineral lamellae contact directly with teeth during friction. The lubricating effect along the longitudinal direction can be markedly enhanced in the brick-and-mortar composites by the presence of intralayer polymer lubricant between mineral bricks. The polymer phase between mineral layers plays an additional role in reducing the contact area between the mineral phase and the tooth antagonists, compared to the transverse configuration, thereby leading to a decreased CoF.

Scanning electron microscopy (SEM) observations clearly reveal different wear damage behavior and micromechanisms of antagonist teeth against 3Y-TZP and nacre-mimetic composites (Figure 2e). The teeth contacting the 3Y-TZP ceramic display an excessive abrasion characterized by abundant wear debris and sharp ploughed furrows parallel to the sliding direction. The enamel prisms frequently break by splitting along their interfaces and de-bonding from their associated mineral nanoparticles (inset). By comparison, wear scratches and debris become much less evident in the antagonist teeth of the nacre-mimetic composites, suggesting reduced tooth abrasion in conjunction with the lower CoFs. This is presumed to result from the markedly decreased hardness and stiffness of the composites and the introduction of the soft polymer phase—a component which causes slight tooth damage as compared to mineral but plays an additional role as a lubricant. The mitigated tooth abrasion with the polymer is clearly revealed by the zigzag end boundaries of the wear tracks for the longitudinal configuration of the lamellar composites. The deep scars and their interspaces with less material loss are caused, respectively, by the mineral lamellae and the polymer phase between them. Of note here is that, at present, a quantitative comparison of the wear rate and volume is excluded by the limited cycles of sliding motion; this will be addressed in a future study.

The *J*-integral and equivalent *K*-based fracture toughness of these nacre-mimetic composites, as compared to monolithic 3Y-TZP ceramic, are shown in **Figure 3**a,b. Note here that the toughness was measured in such a configuration that the cracks propagate across the layers. This conforms well to the case of chipping fracture which is clinically a major cause of failure in dental materials.[24,51] In contrast to the instantaneous cracking of 3Y-TZP, both composites display stable crack propagation and increasing crack-growth resistance with crack extension as evidenced by the steep rising *R*-curve behavior. The critical *J*-integral fracture toughnesses of the lamellar and brick-and-mortar composites were determined to be ≈1.2 and ≈1.7 kJ m^{-2}, respectively, with a critical crack extension limit of ≈0.4 mm in a strict accordance with the ASTM Standard E-1820.[52] These numbers are ≈4 times and ≈6 times higher than monolithic 3Y-TZP, which is notable as 3Y-TZP is known for its high

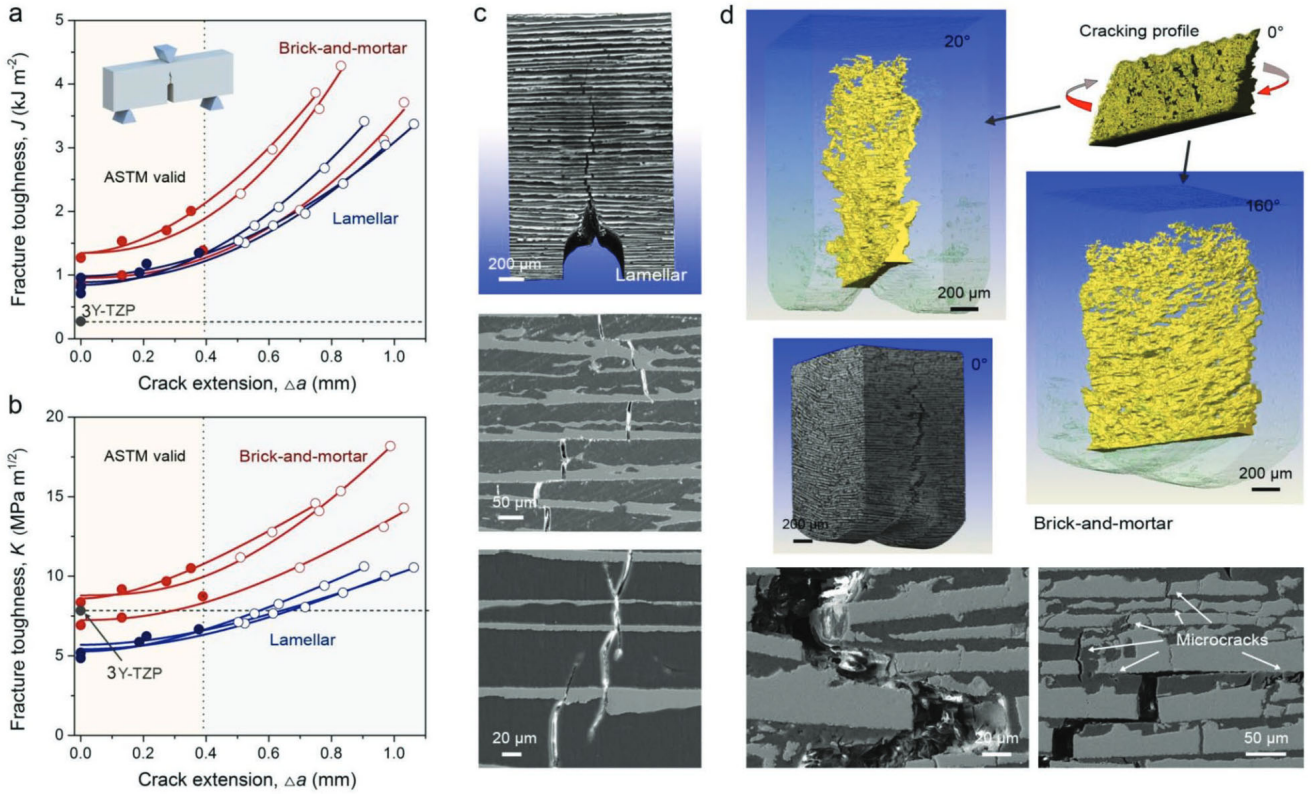

Figure 3. Fracture toughness and toughening mechanisms of nacre-mimetic composites. a) *J*-integral and b) *K*-based fracture toughness with crack extension for the lamellar and brick-and-mortar composites as compared to monolithic 3Y-TZP ceramic. The data, which are strictly ASTM valid, are indicated by solid dots. The inset in panel (a) illustrates the loading configuration of samples for toughness measurement. c,d) XRT renderings and SEM images of crack propagation initiated from a sharpened notch tip in the composites with lamellar (c) and brick-and-mortar (d) architectures. The 3D perspective view of cracking profile was obtained by filtering out the signals from solids (see also Movie S1 in the Supporting Information).

toughness among ceramic materials due to its toughening mechanism mediated by an in situ tetragonal→monoclinic phase transformation.[14,20] The distinctly reduced Young's modulus of the lamellar composites leads to an equivalent *K*-based fracture toughness of ≈6.3 MPa $m^{1/2}$ which is slightly lower than that of 3Y-TZP. In comparison, the brick-and-mortar composites exhibit a crack-initiation toughness (as indicated by the onset of *R*-curve) similar to 3Y-TZP and a critical ASTM valid crack-growth toughness of ≈9.6 MPa $m^{1/2}$, i.e., ≈22% higher than 3Y-TZP.

In situ SEM observations and 3D X-ray tomography (XRT) imaging clearly reveal torturous cracking paths in the composites and a remarkable efficiency of the composite structure in resisting crack propagation (Figure 3c,d). The toughening mechanisms, specifically the effects of the polymer phase and architecture, demonstrate distinct differences between the lamellar and brick-and-mortar composites. The cracks, after penetrating through the polymer layers, tend to deflect along the interfaces between the polymer and mineral constituents in the lamellar composites. The polymer phase plays a role in arresting the cracks through mechanisms of crack-tip blunting and bifurcation; nevertheless, no obvious inelastic deformation of polymer could be detected even with its large layer thickness. In comparison, the brick-and-mortar composites display more a complex cracking profile in 3D space with the cracking paths continuously deflected/twisted along both in-plane and out-of-plane directions, as shown in the perspective view with varying rotations (Movie S1, Supporting Information). The major cracks remain largely intact owing to the bridging effect of the numerous mineral bricks which are present as solid discontinuities in the perspective view. Additionally, the decreased layer thickness of the polymer phase allows for its inelastic deformation and thus enables the controlled shearing between mineral bricks during the pullout of the bridges. The large density of organic–inorganic interfaces further gives rise to abundant microcracks ahead of the major crack tip, which act to promote the formation of crack bridges due to the uncracked ligaments.[53] As such, the enhanced extrinsic toughening mechanisms endow the brick-and-mortar architecture with an improved efficiency in toughening the composites. Additionally, the interfacial enhancement between 3Y-TZP and resin by surface grafting plays a role in promoting the toughening of composites. Such an effect is clearly manifest by the improved fracture toughness and hindered interfacial cracking in grafted composites as compared to those without surface grafting, as shown in Figure S1 in the Supporting Information.

It is of significance, yet still remains a challenge, how intended mechanical properties can be achieved in materials for specific applications. This is particularly pertinent for bioinspired nacre-mimetic composites where the structural

characteristics usually lack a degree of fine modulation. Additionally, despite the implementation of bioinspired designs in mineral–organic composites for structural applications, nacre-like lamellar and brick-and-mortar architectures have rarely been realized in biomedical systems, specifically for dental applications.[39,42–44,54–58] Here, we clarify the architectural design principles of the current composites composed of 3Y-TZP and dental resin in generating their tooth-matching stiffness. The lamellar composites, although having a parallel arrangement of constituents, display a Young's modulus lower than that predicted by the rule-of-mixtures following the Voigt model. This is presumed to result from the fact that around one-fifth (in volume) of the mineral phase extends into the surrounding polymer in form of dendrites or surface asperities of lamellae. We take the effects of such structures into account by assuming an equivalent interlamellar element body comprising the polymer phase with encaged minerals, as illustrated in the inset of Figure 2b. The Young's modulus of the element, E_e, can be approximated as the Reuss-type average of its constituents following the relationship

$$1/E_e = \alpha\phi/\left[(1-\phi+\alpha\phi)E_{3Y\text{-}TZP}\right] + (1-\phi)/\left[(1-\phi+\alpha\phi)E_p\right] \quad (1)$$

where ϕ is the volume fraction of mineral phase in the composites. $E_{3Y\text{-}TZP}$ and E_p represent, respectively, the Young's moduli of the monolithic 3Y-TZP ceramic and polymer phases. The parameter α is the proportion of minerals involved in the hypothetical element; a value of 0.2 is set in the present case. The Young's modulus of the composites, E_c, can then be obtained according to the rule-of-mixtures under an equal-strain assumption of the element and the idealized mineral lamellae, i.e., by excluding the dendrites and asperities, as

$$E_c = (1-\alpha)\phi E_{3Y\text{-}TZP} + (1-\phi+\alpha\phi)E_e \quad (2)$$

As shown in Figure 2b, such a relationship captures well the Young's modulus of the lamellar composites, especially as compared to the Voigt model.

On the other hand, the mineral bricks are largely discontinuous within the unidirectional mineral layers and staggered between adjacent layers in the brick-and-mortar composites. The shear deformation of the interfacial polymer phase is also enabled by its decreased thickness. This offers a principal means for load transfer between the staggered bricks in the composites along the longitudinal direction (inset in Figure 2b). In such a scenario, the Young's modulus of composites can be described, based on the tension–shear chain model which was established in the light of biological composites,[59,60] in terms of the architectural characteristics of the mineral fraction ϕ and the aspect ratio of bricks ρ, following the relationship

$$1/E_c = 4(1-\phi)/\left(G_p\phi^2\rho^2\right) + 1/\left(\phi E_{3Y\text{-}TZP}\right) \quad (3)$$

where G_p represents the shear modulus of the polymer phase. This offers a quantitative rationalization for the modulus of the brick-and-mortar composites (Figure 2b). Therefore, it is essentially from the distinctly nacre-mimetic architectures that the composites develop their specific stiffness.

Figure 4 shows a direct comparison of the mechanical properties of the nacre-mimetic composites with those of dental restorative materials.[7–11,19–23,25–28,30,47–50,61–70] It is clearly seen that the lamellar and brick-and-mortar composites display a remarkable resemblance to human dentin and enamel, respectively, with respect to their hardness, Young's modulus, and flexural strength (representative flexural stress–strain curves are shown in Figure S2 in the Supporting Information). We believe that such good matching with the human tooth, which is unprecedented in any other dental biomaterials reported to date, could lead to dental replacements with markedly improved performance, e.g., by alleviating the stress shielding of neighboring tissue and mitigating the damage and abrasion of opposing teeth. The matching of strength is beneficial for avoiding the premature failure of either tooth replacement or human tooth as they fail at comparable stress levels. As such, it also acts to ensure the normal functions of tooth replacement without facilitating damage to antagonist teeth. Here, we define a parameter η, termed the matching degree, to explicitly quantify the similarity of dental materials to the mechanical performance of human teeth by integrating the above properties. This parameter has the following expression as

$$\eta = \left\{\left[(H_d - H_t)/H_t\right]^2 + \left[(E_d - E_t)/E_t\right]^2 + \left[(\sigma_d - \sigma_t)/\sigma_t\right]^2\right\}^{-1/2} \quad (4)$$

where H, E, and σ denote the hardness, Young's modulus, and strength of materials. The subscripts "d" and "t" indicate properties for the dental materials and human tooth, respectively. The fracture toughness is not included here because higher toughness, rather than to be comparable with that of human tooth, is preferred for dental materials in order to generate better durability and machinability. It is shown that the combinations of mechanical properties for the current composites are the most comparable to those of human teeth, giving the highest level of η (Figure 4d). Note that the matching degree is determined by comparing with human enamel for relatively hard and stiff systems, i.e., ceramics and glass–ceramics, and with human dentin for relatively compliant ceramic–polymer composites.

Our nacre-mimetic composites are additionally distinguished by an exceptional fracture toughness far exceeding the benchmark of most dental materials. Specifically, the lack of architectural designs generally leads to a limited toughness lower than 2.5 MPa $m^{1/2}$ in traditional ceramic–polymer composites for dental applications.[28] The superior damage tolerance of the current composites, in conjunction with the energy-dissipating capability under cyclic loading conditions, is highly favored for enhanced durability of dental replacements to withstand countlessly repeated mastication. Moreover, the moderate hardness and stiffness combined with the high fracture toughness allow for a good machinability of the composites, which is unattainable in the most commonly used 3Y-TZP and other dental ceramics. The brittleness index, as given by the ratio of hardness to fracture toughness,[29,63] gives a direct evaluation on the machinability of dental materials; a lower index signifies better machinability. The current composites demonstrate the lowest brittleness among various dental materials (Figure 4d); this makes it possible for easy manufacturing and processing in a more time- or

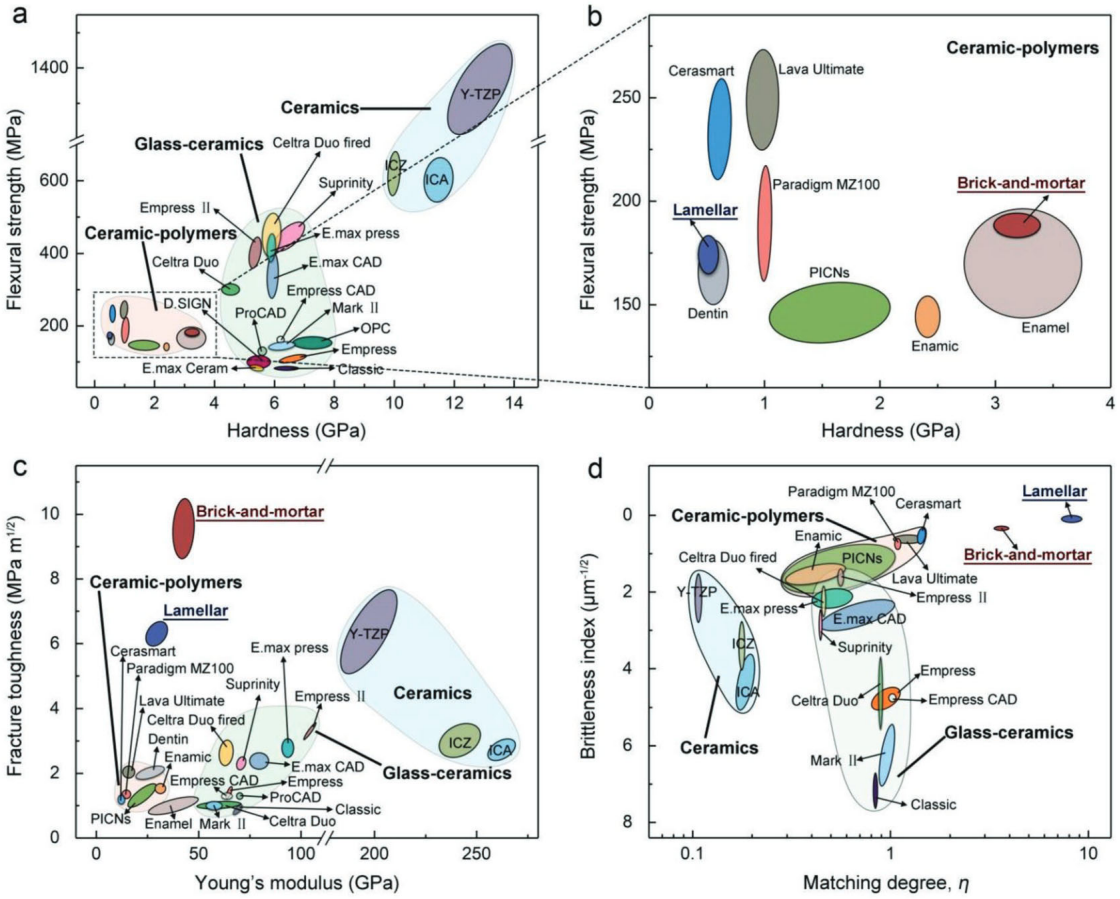

Figure 4. Comparison of nacre-mimetic composites with other dental materials. a,b) Flexural strength and hardness for a wide range of materials for dental applications showing a good resemblance of nacre-mimetic composites with the human tooth.[7–11,19–23,25–28,30,47–50,61–70] b) A magnified view of the dashed box in (a) for ceramic–polymer composites. c) Fracture toughness and Young's modulus of different materials showing human-tooth-matching stiffness and exceptional damage tolerance of the nacre-mimetic composites. d) Matching degree and brittleness index for various materials indicating an unprecedented level of similarity with the human tooth and machinability of the composites.

cost-effective fashion, which contrasts to the personal customized production needed for ceramics. Our preliminary results have shown that these materials can be machined using the computer-aided design and manufacturing (CAD/CAM) method into the desired shape and geometry of dental replacements, as shown in Movie S2 in the Supporting Information.

In summary, we have shown that the hardness, Young's modulus, and strength of human dentin and enamel can be successfully reproduced in novel composites fabricated by infiltrating ceramic scaffolds with a dental resin. The good matching of these properties with those of the human tooth, specifically in terms of stiffness, stems essentially from the nacre-mimetic lamellar and brick-and-mortar architectures which illuminate the principles underlying bioinspired design. These composites are capable of dissipating mechanical energy during cyclic loading and markedly alleviating the abrasion to antagonist teeth, as compared to the performance of monolithic 3Y-TZP ceramics. In particular, the bioinspired designs lead to distinct mechanisms of extrinsic toughening, which are dependent on the specific lamellar and brick-and-mortar architectures, thereby endowing the composites with exceptional damage tolerance. The unprecedented combination of mechanical properties and the excellent machinability suggests that these composites are potential candidate materials for many dental applications as new-generation tooth restorations and replacements. The implementation of bioinspired design principles further opens new possibilities for the creation of more biologically comparable biomaterials with improved performance.

Experimental Section

Fabrication of Lamellar Scaffolds: Bidirectional freeze-casting[42,43] of aqueous suspension of 3Y-TZP powders was employed to produce ceramic scaffolds with lamellar structure. The suspension was prepared by mixing 35 wt% 3Y-TZP nanopowders with a diameter of ≈50 nm (Lifeng Co., China) in deionized water with additions of 0.7 wt% poly(vinyl alcohol) (molecular weight of 84–89 kDa; Meryer Co., China), 0.33 wt% hydroxypropyl methylcellulose (Meryer Co., China), and 0.35 wt% Darvan CN dispersant (R.T. Vanderbilt Co., Norwalk, CT, USA). The organic additives help disperse the ceramic powders, increase the viscosity of slurry to mitigate gravitational sedimentation, and bind the powders after removal of water. The slurry was ball-milled for 48 h and de-aired by adding two drops of defoamer (XP-M-120, Huaxing Co., China) before use. The suspension was poured into square plastic molds (with an inner dimension of 25 × 25 × 70 mm^3) connected to

a copper cold finger which was cooled by immersing one end in liquid nitrogen. PDMS wedges with a slope angle of 25° were equipped at the bottom of molds to create a horizontal temperature gradient in the slurry during the freezing process in addition to the vertical one away from the cold finger.[42,43] The frozen samples were freeze-dried in a vacuum below 5 Pa for at least 64 h, prefired at 500 °C in air for 2 h to remove the organics, and then sintered at 1550 °C for 3 h to form scaffolds with a lamellar structure.

Fabrication of Densified Scaffolds: Ceramic scaffolds with a lamellar structure were prepared by bidirectional freeze-casting of 3Y-TZP suspensions with a solid load of 52 wt% following the procedure described above. After sintering, these scaffolds were infiltrated with paraffin wax and then uniaxially pressed along the normal direction of lamellae with a stress under 600 MPa at 80 °C, i.e., just above the melting point of paraffin wax, to break the mineral lamellae into separate bricks. The melted wax promotes the densification of scaffolds and helps bind the bricks together after its cooling. The densified scaffolds were heat-treated in air at 500 °C for 2 h to burn out the wax and then re-sintered at 1550 °C for 2 h to create interconnections between mineral bricks to form integrity.

Polymer Infiltration of Scaffolds: Nacre-mimetic composites with lamellar and brick-and-mortar architectures were produced by infiltrating the ceramic scaffolds with a light-curing methacrylate resin (ATBIO Co., China) which is clinically used for filling tooth caries. Before infiltration, the scaffolds were surface-grafted with γ-MPS (Chiyechem Co., China) to enhance the interfacial bonding between the organic and inorganic phases. This was realized by immersing the scaffolds in a 20 wt% γ-MPS solution of methanol and water mixture (methanol/water = 9/1 by weight) for 24 h with the pH of solution adjusted to 4 by adding acetic acid. The scaffolds were dried at 40 °C for at least 24 h and then infiltrated with the resin under a negative pressure below 80 kPa in a dark vacuum chamber. The infiltrated scaffolds were exposed to ambient visible light to allow for the curing of resin, and then heat-treated at 40 °C for 3 days and additionally at 90 °C for 2 h to ensure a full polymerization of the monomers. Composites without surface grafting of scaffolds with γ-MPS before infiltration were also prepared for comparison.

Microstructural Characterization: The microstructure of the composites and their morphologies after mechanical testing were characterized by SEM and XRT imaging. SEM imaging was performed using an LEO Supra-35 field-emission scanning electron microscope operating at an accelerating voltage of 20 kV. The samples were sputter-coated with gold before imaging to reduce the charging effect. SEM image analysis was conducted using an Image-Pro Plus 6.0 software. XRT imaging was performed using an Xradia Versa XRM-500 3D X-ray microscope operating at an accelerating voltage of 80 kV. The pixel size of the images was ≈2.4 µm. The results were processed and analyzed using the Avizo Fire 7.1 software.

Mechanical Testing: The mechanical properties of the composites were tested at room temperature in a configuration that the applied stress was parallel to the mineral layers. The hardness was measured on polished samples using an MH-5L Vickers hardness tester with a load of 1 kg and a dwell time of 15 s. Rectangular samples with a cross section of 2 mm × 2 mm and a height of 4 mm were used for the compression tests. Monotonic compression measurements were performed at a constant strain rate of 10^{-3} s^{-1} using an Instron E5982 testing machine (Instron Corp., Norwood, MA, USA) with the displacement monitored by an Instron 2601–92 linear variable differential transformer position sensor. Cyclic compression tests were conducted at displacement-control mode by repeatedly loading and unloading samples at a fixed strain rate of 10^{-3} s^{-1} with constant displacement increase at each cycle. Flexural tests were performed on rectangular beams with a cross section of 2 mm × 1.5 mm and a loading span of 15 mm using an Instron E1000 testing system at a constant displacement rate of 0.1 mm min^{-1}.

In Vitro Wear Testing with a Tooth: Two-body wear tests were conducted in a flat-on-flat contact configuration under artificial saliva lubrication at room temperature using a UNMT-1 Universal nano- and microtester. Rectangular beams of composites with a cross section of 1.5 mm × 1.5 mm were fixed in brass holds and then polished flat to a surface finish of 0.5 µm. Caries-free bovine incisors, with a height of ≈40 mm and a width of ≈15 mm, obtained from a local farm in Shenyang, China, were used as wear antagonists. The labial surfaces of the incisors were embedded flat into an acrylic cold-mounting resin and then ground and polished to a 0.5 µm finish. Reciprocating motion of horizontal sliding at a frequency of 1 Hz was performed on the tooth samples under a vertical load of 1 N for 5000 cycles; the displacement rate and amplitude were fixed at 4 mm s^{-1} and 2 mm, respectively. The load was applied along the mineral layers of the composites with the sliding direction either parallel (*L*) or perpendicular (*T*) to the layers, as illustrated in Figure 2d.

Fracture Toughness Measurement: Single-edge notched bending tests were performed at a constant displacement rate of 3 µm min^{-1} with a loading span of 12.5 mm on a JEOL MicroTest stage inside the chamber of a JEOL JSM-6510 scanning electron microscope. Samples with a width of ≈3 mm and a thickness of ≈1.5 mm were notched at one edge using a water-cooled, low-speed diamond saw with the notch tip sharpened with a razor blade. The load was applied in a configuration that the cracks propagate perpendicular to the mineral layers. The fracture toughness was evaluated in terms of nonlinear elastic fracture mechanics by quantifying the *J*-integral as a function of crack extension, Δa, which was monitored in situ in the SEM. The *J*-integral represents the change in rate of potential energy per unit increase of crack area under nonlinear elastic conditions, and can be obtained for pure bending by $J = (1.9A)/Bb$, where *A* is the total area under load–displacement curve, *b* is the uncracked ligament length, and *B* is the thickness of sample. The fracture toughness based on stress intensity factor, *K*, can be back-calculated from *J* measurements for mode I fracture in plane strain according to $J = K^2/E'$ with $E' = E/(1 - \nu^2)$, where *E* is the Young's modulus and ν is the Poisson's ratio.

Supporting Information

Supporting Information is available from the Wiley Online Library or from the author.

Acknowledgements

This work was financially supported by the National Natural Science Foundation of China (Grant Nos. 51871216 and 51501190). Support for R.O.R. was provided by the U.S. Air Force Office of Scientific Research, under MURI grant AFSOR-FA9550-15-1-0009 to the University of California Riverside through a subcontract to the University of California Berkeley.

Conflict of Interest

The authors declare no conflict of interest.

Author Contributions

Z.L. proposed the idea and designed the experiments. G.T. and J.Z. performed experiments about composite fabrication, microstructural characterization, and mechanical testing. G.T. and L.Z. performed wear tests. D.J. performed fracture toughness measurements. G.T. and Z.L. analyzed the data and wrote the paper. R.O.R. and Z.Z. supervised on the study, discussed the results, and revised the manuscript.

Keywords

bioinspiration, composites, elasticity, fracture toughness, teeth

Received: July 18, 2019
Revised: October 24, 2019
Published online:

[1] M. A. Meyers, P. Y. Chen, A. Y. M. Lin, Y. Seki, *Prog. Mater. Sci.* **2008**, *53*, 1.
[2] F. Barthelat, Z. Yin, M. J. Buehler, *Nat. Rev. Mater.* **2016**, *1*, 16007.
[3] Z. Liu, M. A. Meyers, Z. Zhang, R. O. Ritchie, *Prog. Mater. Sci.* **2017**, *88*, 467.
[4] P. Fratzl, R. Weinkamer, *Prog. Mater. Sci.* **2007**, *52*, 1263.
[5] Z. Liu, Z. Zhang, R. O. Ritchie, *Adv. Mater.* **2018**, *30*, 1705220.
[6] S. Ling, D. L. Kaplan, M. J. Buehler, *Nat. Rev. Mater.* **2018**, *3*, 18016.
[7] B. R. Lawn, J. J. W. Lee, H. Chai, *Annu. Rev. Mater. Res.* **2010**, *40*, 55.
[8] K. J. Koester, J. W. Ager, R. O. Ritchie, *Biomaterials* **2008**, *29*, 1318.
[9] J. J. Kruzic, R. K. Nalla, J. H. Kinney, R. O. Ritchie, *Biomaterials* **2003**, *24*, 5209.
[10] V. Imbeni, J. J. Kruzic, G. W. Marshall, S. J. Marshall, R. O. Ritchie, *Nat. Mater.* **2005**, *4*, 229.
[11] D. Bajaj, D. D. Arola, *Biomaterials* **2009**, *30*, 4037.
[12] Z. Liu, Z. Weng, Z. Zhai, N. Huang, Z. Zhang, J. Tan, C. Jiang, D. Jiao, G. Tan, J. Zhang, X. Jiang, Z. Zhang, R. O. Ritchie, *Acta Biomater.* **2018**, *81*, 267.
[13] H. Chai, J. J. W. Lee, P. J. Constantino, P. W. Lucas, B. R. Lawn, *Proc. Natl. Acad. Sci. USA* **2009**, *106*, 7289.
[14] I. Denry, J. R. Kelly, *Dent. Mater.* **2008**, *24*, 299.
[15] I. Denry, J. R. Kelly, *J. Dent. Res.* **2014**, *93*, 1235.
[16] J. R. Kelly, *Annu. Rev. Mater. Sci.* **1997**, *27*, 443.
[17] R. DeLong, C. Sasik, M. R. Pintado, W. H. Douglas, *Dent. Mater.* **1989**, *5*, 266.
[18] J. D. Hudson, G. R. Goldstein, M. Georgescu, *J. Prosthet. Dent.* **1995**, *74*, 647.
[19] R. G. Luthardt, M. Holzhüter, O. Sandkuhl, V. Herold, J. D. Schnapp, E. Kuhlisch, M. Walter, *J. Dent. Res.* **2002**, *81*, 487.
[20] C. Piconi, G. Maccauro, *Biomaterials* **1999**, *20*, 1.
[21] R. G. Craig, F. A. Peyton, *J. Dent. Res.* **1958**, *37*, 661.
[22] H. H. K. Xu, D. T. Smith, S. Jahanmir, E. Romberg, J. R. Kelly, V. P. Thompson, E. D. Rekow, *J. Dent. Res.* **1998**, *77*, 472.
[23] M. Guazzato, K. Proos, L. Quach, M. V. Swain, *Biomaterials* **2004**, *25*, 5045.
[24] H. J. Conrad, W. J. Seong, I. J. Pesun, *J. Prosthet. Dent.* **2007**, *98*, 389.
[25] J. B. Quinn, V. Sundar, I. K. Lloyd, *Dent. Mater.* **2003**, *19*, 603.
[26] N. D. Ruse, M. J. Sadoun, *J. Dent. Res.* **2014**, *93*, 1232.
[27] B. R. Lawn, A. Pajares, Y. Zhang, Y. Deng, M. A. Polack, I. K. Lloyd, E. D. Rekow, V. P. Thompson, *Biomaterials* **2004**, *25*, 2885.
[28] L. He, M. Swain, *Dent. Mater.* **2011**, *27*, 527.
[29] D. Chaysuwan, K. Sirinukunwattana, K. Kanchanatawewat, G. Heness, K. Yamashita, *Dent. Mater. J.* **2011**, *30*, 358.
[30] A. Coldea, M. V. Swain, N. Thiel, *Dent. Mater.* **2013**, *29*, 419.
[31] A. R. Studart, *Adv. Mater.* **2012**, *24*, 5024.
[32] S. Deville, E. Saiz, R. K. Nalla, A. P. Tomsia, *Science* **2006**, *311*, 515.
[33] H. Zhao, Z. Yang, L. Guo, *NPG Asia Mater.* **2018**, *10*, 1.
[34] U. G. K. Wegst, H. Bai, E. Saiz, A. P. Tomsia, R. O. Ritchie, *Nat. Mater.* **2015**, *14*, 23.
[35] F. Bouville, E. Maire, S. Meille, B. Van de Moortèle, A. J. Stevenson, S. Deville, *Nat. Mater.* **2014**, *13*, 508.
[36] S. Keten, Z. Xu, B. Ihle, M. J. Buehler, *Nat. Mater.* **2010**, *9*, 359.
[37] L. J. Bonderer, A. R. Studart, L. J. Gauckler, *Science* **2008**, *319*, 1069.
[38] B. Yeom, T. Sain, N. Lacevic, D. Bukharina, S. H. Cha, A. M. Waas, E. M. Arruda, N. A. Kotov, *Nature* **2017**, *543*, 95.
[39] E. Munch, M. E. Launey, D. H. Alsem, E. Saiz, A. P. Tomsia, R. O. Ritchie, *Science* **2008**, *322*, 1516.
[40] R. Menig, M. H. Meyers, M. A. Meyers, K. S. Vecchio, *Acta Mater.* **2000**, *48*, 2383.
[41] H. D. Espinosa, J. E. Rim, F. Barthelat, M. J. Buehler, *Prog. Mater. Sci.* **2009**, *54*, 1059.
[42] H. Bai, F. Walsh, B. Gludovatz, B. Delattre, C. Huang, Y. Chen, A. P. Tomsia, R. O. Ritchie, *Adv. Mater.* **2016**, *28*, 50.
[43] H. Bai, Y. Chen, B. Delattre, A. P. Tomsia, R. O. Ritchie, *Sci. Adv.* **2015**, *1*, e1500849.
[44] M. E. Launey, E. Munch, D. H. Alsem, H. B. Barth, E. Saiz, A. P. Tomsia, R. O. Ritchie, *Acta Mater.* **2009**, *57*, 2919.
[45] M. Abboud, M. Turner, E. Duguet, M. Fontanille, *J. Mater. Chem.* **1997**, *7*, 1527.
[46] D. Jiao, Z. Liu, Y. Zhu, Z. Weng, Z. Zhang, *Mater. Sci. Eng., C* **2016**, *68*, 9.
[47] J. W. Stanford, K. V. Weigel, G. C. Paffenbarger, W. T. Sweeney, *J. Am. Dent. Assoc., JADA* **1960**, *60*, 746.
[48] H. Ryou, E. Romberg, D. H. Pashley, F. R. Tay, D. Arola, *J. Mech. Behav. Biomed. Mater.* **2012**, *7*, 3.
[49] J. H. Kinney, M. Balooch, S. J. Marshall, G. W. Marshall, T. P. Weihs, *Arch. Oral Biol.* **1996**, *41*, 9.
[50] J. W. Stanford, G. C. Paffenbarger, J. W. Kumpula, W. T. Sweeney, *J. Am. Dent. Assoc., JADA* **1958**, *57*, 487.
[51] M. V. Swain, *Acta Biomater.* **2009**, *5*, 1668.
[52] ASTM E1820-13, *Standard Test Method for Measurement of Fracture Toughness*, American Society for Testing and Materials International, West Conshohocken, PA, USA **2013**.
[53] J. K. Shang, R. O. Ritchie, *Metall. Trans. A* **1989**, *20*, 897.
[54] Z. Yin, F. Hannard, F. Barthelat, *Science* **2019**, *364*, 1260.
[55] H. Zhao, Y. Yue, L. Guo, J. Wu, Y. Zhang, X. Li, S. Mao, X. Han, *Adv. Mater.* **2016**, *28*, 5099.
[56] M. Grossman, F. Bouville, F. Erni, K. Masania, R. Libanori, A. R. Studart, *Adv. Mater.* **2017**, *29*, 1605039.
[57] Y. Zhang, F. M. Heim, J. L. Bartlett, N. Song, D. Isheim, X. Li, *Sci. Adv.* **2019**, *5*, eaav5577.
[58] H. Zhao, L. Guo, *Adv. Mater.* **2017**, *29*, 1702903.
[59] B. Ji, H. Gao, *J. Mech. Phys. Solids* **2004**, *52*, 1963.
[60] H. Gao, B. Ji, I. L. Jäger, E. Arzt, P. Fratzl, *Proc. Natl. Acad. Sci. USA* **2003**, *100*, 5597.
[61] C. M. Gorman, W. E. McDevitt, R. G. Hill, *Dent. Mater.* **2000**, *16*, 389.
[62] N. C. Lawson, R. Bansal, J. O. Burgess, *Dent. Mater.* **2016**, *32*, e275.
[63] A. R. Boccaccini, *J. Mater. Process. Technol.* **1997**, *65*, 302.
[64] M. V. Swain, A. Coldea, A. Bilkhair, P. C. Guess, *Dent. Mater.* **2016**, *32*, 34.
[65] R. Badawy, O. El-Mowafy, L. E. Tam, *Dent. Mater.* **2016**, *32*, 847.
[66] S. E. Elsaka, A. M. Elnaghy, *Dent. Mater.* **2016**, *32*, 908.
[67] M. Guazzato, M. Albakry, S. P. Ringer, M. V. Swain, *Dent. Mater.* **2004**, *20*, 449.
[68] M. Guazzato, M. Albakry, M. V. Swain, J. Ironside, *Int. J. Prosthodont.* **2002**, *15*, 339.
[69] M. Hayashi, E. V. Koychev, K. Okamura, A. Sugeta, C. Hongo, K. Okuyama, S. Ebisu, *J. Dent. Res.* **2008**, *87*, 762.
[70] S. Bechtle, H. Özcoban, E. T. Lilleodden, N. Huber, A. Schreyer, M. V. Swain, G. A. Schneider, *J. R. Soc., Interface* **2012**, *9*, 1265.